Finger Vein Image Deblurring Using Neighbors-based Binary-GAN (NB-GAN)

He, Jing; Shen, Lei; Yao, YuDong; Wang, HuaXia; Zhao, GuoDong; Gu, Xiaowei; Ding, Weiping

Published in:
IEEE Transactions on Emerging Topics in Computational Intelligence

Publication date:
2021

Citation for published version (APA):
He, J., Shen, L., Yao, Y., Wang, H., Zhao, G., Gu, X., & Ding, W. (Accepted/In press). Finger Vein Image Deblurring Using Neighbors-based Binary-GAN (NB-GAN). *IEEE Transactions on Emerging Topics in Computational Intelligence*.

Finger Vein Image Deblurring Using Neighbors-based Binary-GAN (NB-GAN)

Jing He, Lei Shen, Yudong Yao, *Fellow, IEEE*, Huaxia Wang, *Member, IEEE*, Guodong Zhao, Xiaowei Gu, and Weiping Ding, *Senior Member, IEEE*

***Abstract*—Vein contraction and venous compression typically caused by low temperature and excessive placement pressure can blur the captured finger vein images and severely impair the quality of extracted features. To improve the quality of captured finger vein image, this paper proposes a 26-layer generator network constrained by Neighbors-based Binary Patterns (NBP) texture loss to recover the clear image (guessing the original clear image). Firstly, by analyzing various types and degrees of blurred finger vein images captured in real application scenarios, a method to mathematically model the local and global blurriness using a pair of defocused and mean blur kernels is proposed. By iteratively and alternatively convoluting clear images with both kernels in a multi-scale window, a polymorphic blur training set is constructed for network training. Then, NBP texture loss is used for training the generator to enhance the deblurring ability of the network on images. Lastly, a novel network structure is proposed to retain more vein texture feature information, and two residual connections are added on both sides of the residual module of the 26-layer generator network to prevent degradation and overfitting. Theoretical analysis and simulation results show that the proposed neighbors-based binary-GAN (NB-GAN) can achieve better deblurring performance than the the-state-of-the-art approaches.**

***Index Terms*—Finger vein, GAN, image deblurring, texture loss**

I. Introduction

IMAGE deblurring technology plays an extremely important role in finger vein recognition. During the process of finger vein image acquisition, finger vein contraction caused by low temperature, excessive placement pressure, and equipment instability (i.e., over exposure, defocus, etc.) are the main cause of blurriness of the captured finger vein image [1]. Fig. 1 (a) is a clear finger vein image, and Fig. 1 (b) is a blurred image of Fig. 1 (a). It can be observed that the vein texture of Fig. 1 (b) is seriously blurred, which can greatly deteriorate the meaningfulness of the extracted features [2]. In real application scenarios, the captured finger vein images always exhibit a certain degree of blurriness due to various of reasons. Such blurriness cannot be easily removed by traditional preprocessing techniques and would unfavorably distort the extracted features from affected images as a result of blurred vein textures, significantly deteriorating recognition precision. Hence, image deblurring is the key to perform reliable and robust pattern matching on finger vein images.

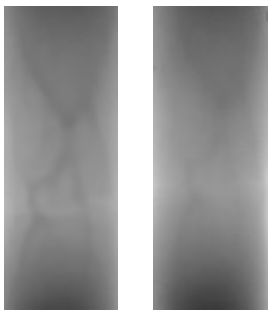

(a) (b)

Fig. 1. Captured finger vein images. (a): Normal clear finger vein image. (b): Blurred finger vein image

Traditional image deblurring algorithms [3-4] attempt to deconvolute blurred image and restore a clear image through utilization of blur kernels. In practice, however, such blur kernels are usually unknown a priori and, thus, these methods cannot be easily applied. The zero-norm prior [5] and the dark channel prior [6] deblurring algorithms consider blurriness to be uniform distributed across the image, and use parametric prior models to estimate the clear image and blur kernel. However, the blurriness of a blurred finger vein image usually is non-uniform distributed across the image in practical. It is very difficult to find a blur kernel that can approximate all types of blurriness in finger vein images. [7] proposed an algorithm for non-uniform deblurring based on parameterized geometric model of the blurring process in terms of the camera's exposure parameters. As these traditional deblurring algorithms need to make prior assumptions about the blur kernel by empirical settings, their generalization ability is usually very low.

Recently, image deblurring algorithms based on deep learning are widely used. [8] and [9] both perform blur kernel estimation steps through Convolutional Neural Networks (CNNs), and then restore clear images by traditional deconvolution methods. [10-12] employ Generative Adversarial Network (GAN) [13-15] to perform the image deblurring task. GAN provides a way for generators and discriminators to fight

Jing He and Lei Shen are with College of Communication Engineering, Hangzhou Dianzi University, Hangzhou 310000, China (e-mail: hdhejing@foxmail.com; shenlei@hdu.edu.cn). *Corresponding author: Lei Shen*

YuDong Yao is with Stevens Institute of Technology, Hoboken, NJ 07030, USA (e-mail: yyao@stevens.edu)

HuaXia Wang is with College of Engineering, Architecture and Technology (CEAT), Oklahoma State University, Stillwater, OK 74078, USA (e-mail: huaxia.wang@okstate.edu)

GuoDong Zhao is with Top Glory Tech Limited Company, Hangzhou 310000, China (e-mail:zhaogd@sdkeji.com)

Xiaowei Gu is with Department of Computer Science, Aberystwyth University, Aberystwyth, SY23 3DB, UK (e-mail: xig4@aber.ac.uk)

Weiping Ding is with School of Information Science and Technology, Nantong University, Nantong, 226019, China (e-mail: ding.wp@ntu.edu.cn)

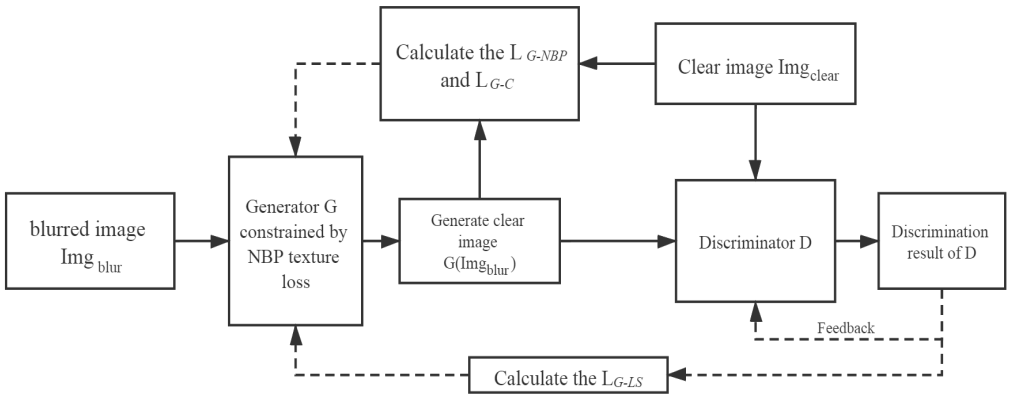

Fig. 2. The structure of the proposed NB-GAN

against each other, in order to learn the mapping relationship between blurred images and clear images. Through the well trained generator, deblurred images can be output directly, achieving better deblurring results than CNN. [16] proposes an image deblurring algorithm based on Deblurring Generative Adversarial Networks (DeblurGAN). DeblurGAN adds additional information such as tags on top of GANs, which can generate the desired samples more accurately. In addition, DeblurGAN uses the residual network architecture in the generator, which can extract more texture edge information and achieve better results deblurring performance. The aforementioned algorithms use the difference in gray value between clear and deblurred image as generator loss. For finger vein images with blurred texture (i.e., low resolution, less vein information, low contrast between vein and background), it is far more challenging to remove the blurriness completely due to: 1) the lack of constraints on the vein texture. 2) the down-sampling will cause loss of key vein texture information.

In this paper, a novel approach based on a 26-layer generator network constrained by Neighbors-based Binary Patterns (NBP) texture loss is proposed for finger vein images deblurring. This research firstly investigates the blur characteristics of blurred finger vein images captured in real-world scenario, and proposes the mathematical expressions of local and global blurriness of finger vein images. Based on this, synthetic images with multi-type and multi-degree blurriness are created for training the network and further improving it generalization ability. Secondly, the NBP [17] texture distance between the input image and the generated image is considered as the texture loss function, which can restore the finger vein image with high fidelity. Lastly, considering the feature of less vein information in the blurred finger vein images, an extra residual jump link layer is added to both sides of the residual module of the generator network to enhance the learning ability of the network, preventing model degradation and overfitting.

To summarize, main contributions of this paper include:

1) a method to mathematically model the local and global blurriness of finger vein images;

2) a novel 26-layer generator network with two residual connections constrained by NBP texture loss for image deblurring.

The remainder of the paper is organized as follows. The section II describes the basic principles of NB-GAN proposed in this paper. The section III describes the mathematical model of the blurriness. The section IV describes the composition of NB-GAN network and its loss function. In the section V, how to design the training dataset and testing dataset in this paper are introduced. In the section VI, the effectiveness of the NB-GAN for deblurring is verified in terms of visual effects, Peak Signal-to-Noise Ratio (PSNR) [18] and Structure Similarity (SSIM) [18], and recognition performance. The section VII is the conclusion.

II. Finger Vein Deblurring Algorithm Based on NB-GAN

A. Analysis of Blur Characteristics of Finger Vein Images

Image deblurring is the process of restoring a clear image from the blurred image. The blurred finger veins image can be expressed as follows [19],

$$Img_{\mathrm{blur}} = \boldsymbol{K} \otimes Img_{\mathrm{clear}} \tag{1}$$

where, Img_{blur}, $\boldsymbol{K}$, and Img_{clear} are blurred finger vein image, blur kernel, and latent clear finger vein image, respectively. $\otimes$ denotes the convolution operation. The category of blurriness can be roughly divided into two categories, namely, local blurriness and global blurriness. Local blurriness is mainly caused by excessive placement pressure applied by unskilled people, and global blurriness is mainly due to vein contraction caused by low temperature in winter. Very importantly, the degree of vein contraction caused by low temperature and the degree of vein compression caused by pressure usually differ from person to person, finger to finger. Thus, the blur kernels $\boldsymbol{K}$ of different finger vein can vary significantly.

B. Deblurring Network Based on NB-GAN

The structure of finger vein image deblurring based on NB-GAN proposed by this paper is shown in Fig. 2. The NB-

GAN consists of a 26-layer generator network, G constrained by NBP texture loss and a discriminator network, D. During the training process, Img_{blur} (the blurred image paired with Img_{clear}) is passed to the generator to generate a deblurred image $G(Img_{\mathrm{blur}})$ and then, both $G(Img_{\mathrm{blur}})$ and Img_{clear} are passed to the discriminator network. The discriminator network is trained to classify $G(Img_{\mathrm{blur}})$ to a fake label (i.e., $D(G(Img_{\mathrm{blur}}))=0$) and Img_{clear} to a real label (i.e., $D(Img_{\mathrm{clear}})=1$). Utilizing the NBP texture loss $L_{\mathrm{G-NBP}}$, content loss $L_{\mathrm{G-C}}$, and least square loss $L_{\mathrm{G-LS}}$, the generator network is trained to learn the distribution of clear images until the discriminator network cannot distinguish the Img_{clear} and $G(Img_{\mathrm{blur}})$, which indicates that the parameters of the current network are optimal.

The proposed blurring model is formulated as follows.

$$\begin{aligned}\min_{G}\max_{D} V(D,G) = E_{x\sim p_{\mathrm{r}}(x)}(\log_2 D(x)) \\ +E_{x'\sim p_{\mathrm{g}}(x')}(\log_2(1-D(x')))\end{aligned} \tag{2}$$

where $E(*)$ represents mathematical expectation function. p_{r} is the real data distribution and p_{g} is the model distribution, x is defined as Img_{clear}, x' is defined as $G(Img_{\mathrm{blur}})$.

III. Modelling The Blurriness

To understand the properties of blurriness across finger vein images, this paper categorizes the blurriness into two categories as aforementioned: local blurriness, caused by excessive placement pressure, and global blurriness, caused by vein contraction due to low temperature. The degrees of blurriness caused by various factors are different. Based on the characteristics of finger vein images with multi-type and multi-degree blurriness, this paper proposes a method to mathematically model the blurriness with a pair of defocused and mean blur kernels, which convolute the image iteratively and alternatively in a multi-scale window. The proposed blurring model is as follows,

$$\begin{aligned}\boldsymbol{B}_{n+1}(x,y) = \boldsymbol{B}_n(x,y)\otimes h_n(x,y,l_n)\otimes g_n(x,y,r_n), \\ \frac{R-k_{n,\mathrm{R}}}{2} < x < R-\frac{R-k_{n,\mathrm{R}}}{2}, \\ \frac{C-k_{n,\mathrm{C}}}{2} < y < C-\frac{C-k_{n,\mathrm{C}}}{2}, \\ 0<k_{n,\mathrm{R}}\le R, 0<k_{n,\mathrm{C}}\le C, n\in[0,1,2,...,N-1]\end{aligned} \tag{3}$$

where n is the n^{th} convolution iteration of blur kernel. N is the total number of iterations. x and y are pixel coordinates. R and C are the height and width of the image respectively. $k_{n,\mathrm{R}}$ and $k_{n,\mathrm{C}}$ are the height and width of the convolution window at the n^{th} convolution iteration. $\boldsymbol{B}_n(x,y)$ is the synthetic blurred image after n iterations of the convoluting blur kernel (i.e., $\boldsymbol{B}_0(x,y)$ is the input image). $h_n(x,y,l_n)$ is the defocused blur kernel spread function with radius l_n at the n^{th} convolution iteration, which used to simulate the blur characteristics of vein texture edge. The expression of $h_n(x,y,l_n)$ is written as follows,

$$\begin{aligned}h_n(x,y,l_n) = \begin{cases}\frac{1}{\pi l_n^2}, \sqrt{x^2+y^2}\le l_n \\ 0 \quad ,\text{other}\end{cases}, \\ n\in[0,1,2,...,N-1]\end{aligned} \tag{4}$$

$g_n(x,y,r_n)$ is the mean blur kernel spread function with radius r_n at the n^{th} convolution iteration, which used to simulate the blur characteristics of the overall vein texture and background. The expression of $g_n(x,y,r_n)$ is written as follows,

$$\begin{aligned}g_n(x,y,r_n) = \begin{cases}\frac{1}{(2r_n+1)^2}, |x|\le r_n, |y|\le r_n \\ 0 \quad ,\text{other}\end{cases}, \\ n\in[0,1,2,...,N-1]\end{aligned} \tag{5}$$

By iteratively adjusting the parameters in Eqn. (3)-(5), the proposed blurring model can accurately approximate various blur degrees and blur types. In the follow subsections, the details of the mathematical models of the local blurriness and global blurriness are presented.

A. Modelling the Local Blurriness

For modelling the local blurriness, we set $k_{0,\mathrm{R}}$ and $k_{0,\mathrm{C}}$ as the height and width of the initial window, which is corresponding to the size of the force area obtained by a finger pressure. Different finger collection postures have different sizes of force areas. For the local blurred finger vein image, the degree of blurriness of the force area decrease from the centre to the periphery. In this paper, the height and width of the n^{th} convolution window $k_{n,\mathrm{R}}$ and $k_{n,\mathrm{C}}$ in the convolution process are expanded with n to approximate the gradual diffusion from the force area to the periphery. The calculation expression for the height and width of the convolution window used by Eqn. (3) is written as follows,

$$\begin{aligned}k_{n,\mathrm{R}} = \lfloor \frac{R-k_{0,\mathrm{R}}}{N-1}n + k_{0,\mathrm{R}} \rfloor, \\ k_{n,\mathrm{C}} = \lfloor \frac{C-k_{0,\mathrm{C}}}{N-1}n + k_{0,\mathrm{C}} \rfloor, \\ n\in[0,1,2,...,N-1]\end{aligned} \tag{6}$$

where $\lfloor * \rfloor$ is the round-down operation.

The radii l_n and r_n of the defocused blur kernel and mean blur kernel are reduced by n times λ_l and λ_r to approximate the gradual decrease of the blur degree from the force area to the periphery. The radii of the defocused blur kernel and mean blur kernel at the n^{th} iteration in Eqn. (3) are defined as follows,

$$\begin{aligned}l_n = \lfloor\ l_0 - \lambda_{\mathrm{l}} n \rfloor, l_n \ge 0, \\ r_n = \lfloor\ r_0 - \lambda_{\mathrm{r}} n \rfloor, r_n \ge 0, \\ n\in[0,1,2,...,N-1]\end{aligned} \tag{7}$$

where, l_0 and r_0 are the initial radii of the defocused blur kernel and the mean blur kernel, respectively. λ_{l} and λ_{r} are the corresponding decreasing rates of two radii for adjusting the diffusion velocity of blur degree in blurred finger vein image during an iterative convoluting process.

In general, this blurring model can approximate the multi-degree local blurriness of finger vein image by adjusting the parameters in Eqn. (3)-(7). The externally controlled parameters include the iteration times N, the initial window size $k_{0,\mathrm{R}}$ and $k_{0,\mathrm{C}}$, the radius size of initial blur kernel l_0 and r_0, and the decreasing rate of blur kernel radius λ_{l} and λ_{r}. Fig. 3 (a) is the image captured under normal pressure. Fig. 3 (b) is the

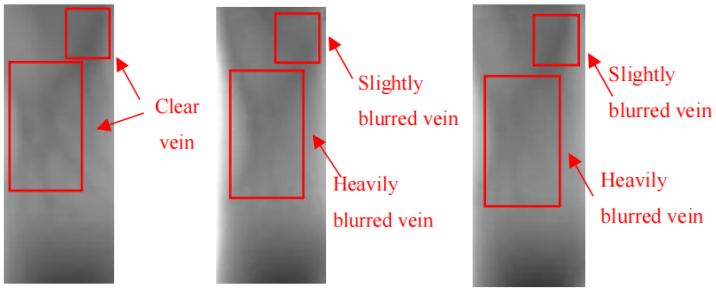

Fig. 3. Local blurred finger vein images. (a): Clear image. (b): Real local blurred image caused by pressing. (c): Synthetic local blurred image generated from Fig. 3 (a).

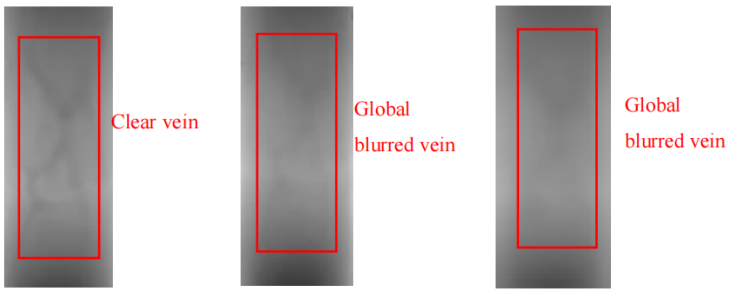

Fig. 4. Global blurred finger vein images. (a): Clear image. (b):Real global blurred image caused by low temperature. (c): Synthetic global blurred image generated from Fig. 4 (a).

image captured by the same finger under heavy pressure. It can be observed that the central force area is more blurred than the periphery. Fig. 3 (c) shows the synthetic local blurred finger vein image with $N = 6$, $n \in [0, 1, ..., 5]$, $k_{0,\mathrm{R}} = 100$, $k_{0,\mathrm{C}} = 40$, $l_0 = 4$, $r_0 = 3$, $\lambda_\mathrm{l} = 0.4$, $\lambda_\mathrm{r} = 0.4$. Comparing with Fig. 3 (b) with Fig. 3 (c), one can see that the blurred features of the local blurred finger vein image simulated by this model are well consistent with the real local blurred finger vein images.

B. Modelling the Global Blurriness

For the global blurriness, the height and width of convolution window should be fixed as the input image height and width. Thus, the height $k_{n,\mathrm{R}}$ and width $k_{n,\mathrm{C}}$ of convolution window in Eqn. (3) should be constants. Eqn. (6) can be rewritten as follows:

$$\begin{aligned} k_{n,\mathrm{R}} = R, k_{n,\mathrm{C}} = C, \\ n \in [0, 1, 2, ..., N-1] \end{aligned} \tag{8}$$

The global blurriness can be approximated by reducing the radius l_n and r_n of the blur kernel in the convolution process. The calculation formula of the radius of the global blur kernel is the same as the local blur kernel given by Eqn. (7).

In short, the multi-degree global blurriness of the finger vein image can be simulated by adjusting the parameters in Eqn. (3, 4, 5, 7). The parameter details are the iteration number N, the initial radius of blur kernel l_0 and r_0, and the reduction rate of the radius of the blur kernel λ_l and λ_r. Fig. 4 (a) shows the finger vein images captured when the temperature is normal in summer. Fig. 4 (b) shows the image of the same finger when the temperature is cold in winter. Through observation, we can see that all vein textures in Fig. 4 (b) are very blurred. Fig. 4 (c) is a global blurred finger veins image simulated by the proposed method with the parameters $N = 5$, $n \in [0, 1, ...4]$, $l_0 = 4$, $r_0 = 4$, and $\lambda_\mathrm{l} = 0.5$, $\lambda_\mathrm{r} = 0.4$. Comparing Fig. 4 (c) and Fig. 4 (b), one can see that the global blurred finger veins image simulated by this model is well consistent with the blurred finger vein image caused by vein contraction in low temperature.

As shown by the analysis presented in this section, a synthetic blurred finger vein image can be obtained by using a pair of defocused and mean blur kernels to convolute clear finger vein image iteratively and alternatively in a multi-scale window. In the section IV, a deblurring model based on NB-GAN will be established according to the blur features of finger vein image analyzed above.

It has to be admitted that as there is no paired images available, it is not possible to calculate the PSNR and SSIM for the examples presented in Figs. 3 and 4. Thus, the quality of the synthesized images is evaluated empirically by visual judgement. However, the numerical experiments presented in Section VI show that the performance of the deblurring model can be largely improved by training with the synthetic blurred images generated based on the proposed blurring model in this paper, proving its efficacy.

Note that in a typical finger vein recognition system, noises caused by the scar tissue, incision or hair are very different from the vein texture on the finger vein images, and it will not develop into an artificial vein pattern, nor affect recognition performance. Thus, the influence of such types of noises is

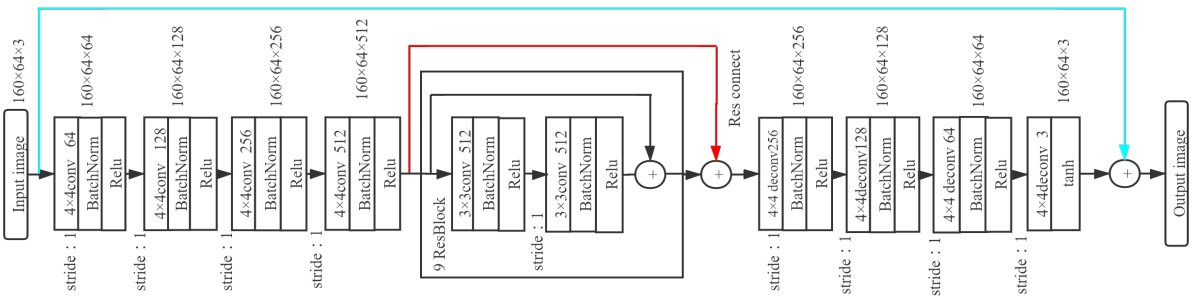

Fig. 5. Architecture of 26-layer NB-GAN generator network

not considered in this study. There have been some methods proposed recently [20-21] to remove noises from the captured finger vein images.

IV. Deblurring Network Model of Finger Vein Image Based on NB-GAN

The core idea of the deblurring model based on NB-GAN is the zero-sum game, namely, if one side gains during the game, the other side will lose, correspondingly, and the sum of the losses and gains of the two sides will always be equal to zero. The two sides of the game are generator network and discriminator network. The main task of the generator network is to learn the mapping relationship between the blurred image and the clear image until the Nash equilibrium, namely, the discriminator network cannot distinguish the generated image from the real image. The main task of the discriminator network is to judge whether the input image is a deblurred image or a clear image, and to game with the generator network.

A. Network Structure of NB-GAN Generator Network

The architecture of the NB-GAN 26-layer generator network used in this research is shown in Fig. 5, which follows a similar setting as given in [16]. As one can see from this figure, the generator network is composed of four 4×4 convolution blocks, 9 residual blocks (ResBlock), and 4 deconvolution blocks. Each ResBlock is composed of two 3×3 convolutional layers. The multi-layer residual structure can effectively refine the learned vein features and improve the overall recognition accuracy.

In this paper, we set stride step to be 1 for convolution to increase the information content of vein texture features. A 4×4 convolution kernel is used to enhance the receptive field of texture features. The 26-layer architecture is used to enhance the learning ability of the network with the aim of restoring clearer texture vein image using the extracted vein texture features. In order to effectively prevent model degradation and over fitting, and accelerate network convergence, a residual jump connection and a global residual connection are added in the generator network. The residual jump connection is represented by the red line shown in Fig. 5. Residual jump connection can make full use of the finger vein image information of shallow network to prevent model degradation and overfitting, achiveing better deblurring performance. The global connection is the blue line shown in Fig. 5. The global residual connection enables the network to learn only the residual between the input image and the generated image, thus making the network converge faster.

B. Network Structure of NB-GAN Discriminator Network

The accuracy of the discriminator network will directly affect the performance of the generator network. To ensure that the vein texture details of the generated image are clear, this paper uses the Markovian Patch Discriminator [22] as the discriminator network structure. The network structure is composed of five 4×4 convolution blocks, as shown in Fig. 6.

The discriminator network randomly divides a input image into several $H \times W$ image blocks. Each image block outputs a value through the network, and then takes the average of all output values as the final discrimination result. In the training process, it can pay more attention to the local characteristics of the vein image, resulting in clearer vein texture details of the generated image. Based on the width of the finger vein texture, in our experiment, we set $H = 10$, $W = 4$.

C. Loss Function of NB-GAN

The NB-GAN training itself is a min-max optimization process. The main aim of the two sub networks (namely, generator and discriminator) is to maximize the other's loss function and minimize its own loss function. Once converged, the image generated by the generator is closer to the practical clear image.

The NB-GAN loss contains a discriminator loss function and a generator loss function.

1) Discriminator Loss: Due to the lack of information in finger vein blurred image, the gradient may disappear too fast in the training process, which will lead to the insufficient learning of texture features by the network, and the restored image still has texture blur. In this paper, we propose to use the least square loss function as the discriminator loss, which effectively solves the problem of gradient vanishing and enables the network to better learn the vein texture feature

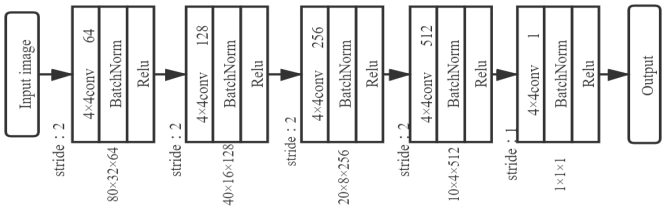

Fig. 6. Architecture of NB-GAN discriminator network

[23]. The discriminator loss L_{D} of the NB-GAN is defined as follows,,

$$L_{\mathrm{D}} = \frac{1}{2}E_{Img_{\mathrm{clear}}\sim p_{\mathrm{c}}}[(D(Img_{\mathrm{clear}})-1)^2]+ \frac{1}{2}E_{Img_{\mathrm{blur}}\sim p_{\mathrm{b}}}[(D(G(Img_{\mathrm{blur}})))^2] \tag{9}$$

where $Img_{\mathrm{clear}} \sim p_{\mathrm{c}}$ means that Img_{clear} is taken from the vein clear image set p_{c}, and $Img_{\mathrm{blur}} \sim p_{\mathrm{b}}$ means that Img_{blur} is taken from the vein blurred image set p_{b}.

2) Generator Loss: To improve the fidelity and texture clarity of the restored finger vein image, and ensure that the background area of the restored finger vein image is smooth and closer to the practical clear finger vein image, we combine the local texture feature loss, content loss, and least square loss in the generator loss, which can be expressed as follows,

$$L_{\mathrm{G}} = \lambda_1 L_{\mathrm{G-NBP}} + \lambda_2 L_{\mathrm{G-C}} + \lambda_3 L_{\mathrm{G-LS}}, \quad \lambda_1+\lambda_2+\lambda_3 = 1 \tag{10}$$

where $L_{\mathrm{G-NBP}}$, $L_{\mathrm{G-C}}$, and $L_{\mathrm{G-LS}}$ denote local texture loss, content loss, and least square loss, respectively. In order to prevent content loss weight from causing excessive sharpening of the image and affecting the extraction of vein texture features, $\lambda_1 = 0.4$, $\lambda_2 = 0.2$, and $\lambda_3 = 0.4$. The detail loss function are explained as follow.

(1) *Local Texture Loss*

In order to improve the fidelity of restored finger vein image, the local NBP features [17] of finger vein images are proposed to describe the vein texture structures, and the Hamming distances between the NBP features of the paired real clear images and the deblurred images is taken as a part of the loss function used by generator. NBP has good local feature description characteristics. This can help the generator network to learn the texture details of the clear vein image more accurately, ensuring the similarity between the structures of the input image and the deblurred image. Because of the thin texture of finger vein, the NBP operator of 3×3 window is used in this paper. Let (x, y) be a particular pixels on the image Img. Starting from the upper left of the window, the eight pixels around (x, y) are numbered as $p_0, p_1, ...p_7$. NBP feature extraction function NBP (*) is formulated as follows.

$$NBP(Img) = \sum_{i=0}^{7} s_i \cdot 2^i,$$
$$s_i = \begin{cases} 1, p_{i+1} - p_i > 0 \\ 0, p_{i+1} - p_i \le 0 \end{cases}, \qquad i = 0, 1, 2...6, \tag{11}$$
$$s_7 = \begin{cases} 1, p_0 - p_7 > 0 \\ 0, p_0 - p_7 \le 0 \end{cases}$$

The NBP texture loss function is formulated as follows,

$$L_{\mathrm{G-NBP}} = \frac{1}{8TRCM}\sum_{m=1}^{M} Hamm(NBP(G(Img^m_{\mathrm{blur}})), NBP(Img^m_{\mathrm{clear}})) \tag{12}$$

where T is the number of channels, R is the height of the image, C is the width of the image. Img^m represents the m^{th} image, and M is the number of images. $Hamm(*)$ is the Hamming distance calculation function.

(2) *Content Loss*

In real application scenarios, the camera of the finger vein image acquisition equipment is usually prone to high exposure, resulting in abnormal pixel at the edge of the captured image. This can seriously affect the training result of network model, leading to poor deblurring performance. To address this problem, this paper uses Mean Absolute Error (MAE, also known as ℓ^1) loss as the content loss. ℓ^1 loss will ignore some outliers in the training process leading to better deblurring performance [22]. The ℓ^1 loss function is expressed as follows.

$$L_{\mathrm{G-C}} = \frac{1}{TRCM}\sum_{m=1}^{M} |G(Img^m_{\mathrm{blur}}) - Img^m_{\mathrm{clear}}| \tag{13}$$

(3) *Least Squares Loss*

To tackle the problem of gradient vanishing during the training process and ensure the full learning of vein texture information, we also add the least square loss [23] to the generator loss, in which is defined as follows:

$$L_{\mathrm{G-LS}} = \frac{1}{2}E_{Img_{\mathrm{blur}}\sim p_{\mathrm{b}}}[(D(G(Img_{\mathrm{blur}}))-1)^2] \tag{14}$$

V. Dataset Description

The finger vein image acquisition device used in this study (as shown in Fig. 7 (a)) is a cutting-edge device that has been widely put into commercialization. There is a sensor in

TABLE I
THE PARAMETER DETAILS OF SYNTHETIC SINGLE-BLUR-DEGREE TRAINING DATASET

Blur categories	N	$k_{0,\mathrm{R}} \times k_{0,\mathrm{C}}$	l_0	λ_l	r_0	λ_r	Blur types	Images number
Local blur	5:1:6	80×32:10×4:120×48	4	0.4	3	0.3	10	960
Global blur	5:1:6	300×200	4	0.4	3	0.3	2	960

TABLE II
THE PARAMETER DETAILS OF SYNTHETIC POLYMORPHIC TRAINING DATASET

Blur categories	N	$k_{0,\mathrm{R}} \times k_{0,\mathrm{C}}$	l_0	λ_l	r_0	λ_r	Blur types	Images number
Local blur	5:1:7	80×32:10×4:120×48	4:1:5	0.4:0.1:0.5	3:1:4	0.3:0.1:0.4	240	960
Global blur	5:1:7	300×200	4:1:5	0.4:0.1:0.5	3:1:4	0.3:0.1:0.4	48	960

TABLE III
THE PARAMETER DETAILS OF SYNTHETIC BLURRED TESTING DATASET

Blur categories	N	$k_{0,\mathrm{R}} \times k_{0,\mathrm{C}}$	l_0	λ_l	r_0	λ_r	Blur types	Images number
Local blur	5:1:8	80×32:10×4:120×48	4:1:5	0.3:0.1:0.5	3:1:4	0.3:0.05:0.4	720	720
Global blur	5:1:8	300×200	4:1:5	0.3:0.1:0.5	3:1:4	0.3:0.05:0.4	144	720

TABLE IV
THE COMPOSITION OF REAL BLURRED FINGER VEIN IMAGES TESTING DATASET

Real scene	Fingers number	Images number
Excessive pressure (real local blur)	60	600
Normal pressure	60	600
Winter (real global blur)	100	1000
Summer	100	1000

the groove of this device, and the finger vein image can be captured by placing the finger in the groove. However, one has to raise the finger to reactivate the sensor when repeatedly capturing images, which will inevitably lead to a certain degree horizontal or vertical displacement of the repeatedly captured images. As there is no easy method to capture a large amount of paired clear and blurred finger vein images for one-to-one training, this paper uses the blurring model proposed in section III to construct a synthetic set of image pairs for network training.

To summarize, we use two training datasets to train the proposed NB-GAN deblurring model:

1) a synthetic single-blur-degree training dataset with fewer blur types,

2) a synthetic polymorphic blur training dataset with a large mount of types are addressed.

To verify the effectiveness of the proposed NB-GAN deblurring model, we use three testing dataset:

1) a synthetic blurred testing dataset which consisted of a local blurred dataset and a global blurred dataset,

2) a real local blurred testing dataset caused by finger vein compression due to excessive pressure,

3) a real global blurred testing dataset caused by finger vein contraction due to low temperature.

Tables I $\sim$ III show the specific parameter settings of Eqn. (3)-(8) for generating the synthetic training and testing sets. The size of finger vein images used in this paper are 300×200, and all images were captured by students at HangZhou DianZi University.

A. Training Dataset

As aforementioned, it is impossible to capture a large image set consisted of paired blurred and clear finger vein images for training in practical, this study uses the proposed blurring model to create a paired training dataset through blurring the captured clear finger vein images. The clear finger vein image library for training contains 427 fingers. 1$\sim$3 images were captured for each finger, with 960 images in total. $V_\mathrm{b} : s : V_\mathrm{e}$ means take V_b as the starting value, and increase to the final value V_e with the step size of s.

For generating the synthetic single-blur-degree training dataset, 10 local blur types and two global blur types were considered. We fix the kernel radii as $l_0 = 4$, $r_0 = 3$ and the respective decreasing rates as $\lambda_\mathrm{l} = 0.4$, $\lambda_\mathrm{r} = 0.3$. The specific parameter details are shown in Table I. Two different numbers of iterations N and five different initial convolution window sizes $k_{0,\mathrm{R}} \times k_{0,\mathrm{C}}$ are used to produce the local blurred finger vein dataset. In total, 960 training images of 10 (2×5) different types of local blurriness (96 per type) were generated. Two different N are considered for producing the global blurred finger vein image set. Another 960 training images of two different types of global blurriness (480 per type) are generated.

For generating the synthetic polymorphic blurred training dataset, 240 local blur types and 48 global blur types are considered. The specific parameter details are shown in Table II. Three different N , five different $k_{0,\mathrm{R}} \times k_{0,\mathrm{C}}$, two different l_0, two different λ_l, two different r_0, two different λ_r were used to produce the local blurred finger vein dataset, which consists of 960 images of 240 ($3 \times 5 \times 2 \times 2 \times 2 \times 2$) different types of local blurriness (4 images per type). Then, three different N, two different l_0, two different λ_l, two different

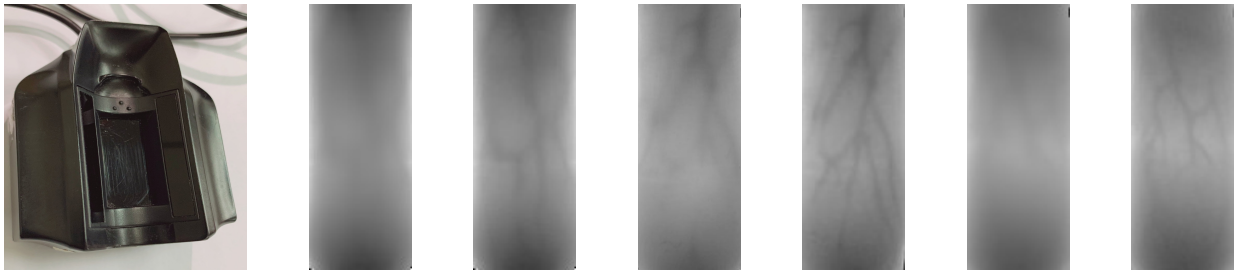

(a) (b) (c) (d) (e) (f) (g)

Fig. 7. Finger vein image acquisition equipment and paired blurred and normal clear finger vein images of the test dataset. (a): Finger vein image acquisition equipment. (b): Synthetic blurred finger vein image. (c): Normal clear image corresponding to Fig. 7(b). (d): Real local blurred finger vein image. (e): Normal clear image corresponding to Fig. 7(d). (f): Real global blurred finger vein image. (g): Normal clear image corresponding to Fig. 7(f).

r_0, two different λ_{r} are used to generate the global blurred finger vein image set, which consists of 960 images of 48 ($3 \times 2 \times 2 \times 2 \times 2$) different types of blurriness (20 images per type).

B. Testing Dataset

This paper uses one synthetic dataset and two real-world datasets captured in real application scenarios to verify the efficacy of the proposed NB-GAN-based deblurring approach.

To generate the synthetic blurred testing dataset, we use the clear image library, which includes 720 images of 72 fingers, 10 images per finger. In total, 720 synthetic local blur images are produced with four different N, five different $k_{0,\mathrm{R}} \times k_{0,\mathrm{C}}$, two different l_0, three different λ_{l}, two different r_0, three different λ_{r}. Each image belongs to a particular blur type, and thus, there are 720 ($4 \times 5 \times 2 \times 3 \times 2 \times 3$) different types of local blurriness. Another 720 synthetic global blur images are generated with four different N, two different l_0, three different λ_{l}, two different r_0, three different λ_{r}. Thus, there is a total of 144 ($4 \times 2 \times 3 \times 2 \times 3$) types of global blurriness (5 images per type). The specific parameter details are shown in Table III. Fig. 7 (b) and Fig. 7 (c) shows a pair of synthetic blurred and normal clear example images.

The real local blurred testing dataset, where the blurriness is caused by finger vein compression, contains 60 fingers, as shown in Table IV. Each finger collects 20 images. Among them, 10 finger vein images captured with excessive pressure, and other 10 finger vein images captured by the same finger with normal pressure, there are 1200 images in total. Fig. 7 (d) and Fig. 7 (e) shows a pair of real local blurred and normal clear example images.

The real global blurred testing dataset, where the blurriness is caused by finger vein contraction in low temperature, contains a total of 2000 finger vein images collected from 100 fingers. Example images are shown in Table IV. Among the 2000 images, half of them are captured during winter (namely, 10 images per finger captured in cold temperatures with vein contraction). The other half are captured by the same finger in summer (namely, 10 clear images per finger captured in normal temperatures). Fig. 7 (f) and Fig. 7 (g) shows a pair of real global blurred and normal clear example images.

VI. Experimental Results

This paper uses Pytorch deep learning framework to perform experiments on a desktop with Ubuntu system and a Nvidia 1080Ti GPU. The training dataset contains 960 images, the training batch size is 16, the number of iterations is 400, the global learning rate is 0.002, and it is optimized by the ADAM optimizer [24]. Neighbors-based Binary Patterns (NBP) [17] recognition simulation is programmed with Matlab R2016a software. The computer is configured as Windows7 64-bit operating system. CPU is Intel (R) Core (TM) i5-6500, clocked at 3.20 GHz, and memory is 4 GB. In this paper, visual evaluation, Peak Signal-to-Noise Ratio (PSNR) [18], Structure Similarity (SSIM) [18], and recognition performance are proposed to evaluate the deblurring algorithm.

The training loss curves of discriminator network and generator network of NB-GAN constrained by NBP texture loss with the polymorphic training dataset are given by Fig. 8. From Fig. 8, it can be observed that the loss values of the discriminator network and the generator network gradually decrease and slowly converges to the locally minimum values as the number of training epochs gradually increases.

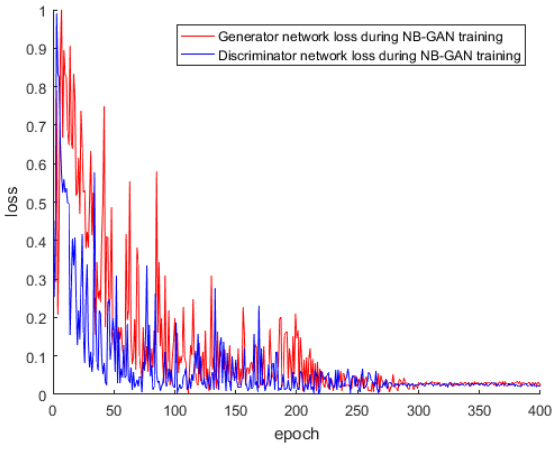

Fig. 8. Loss curve of NB-GAN constrained by NBP texture loss and trained with polymorphic training dataset.

A. Visual Evaluation

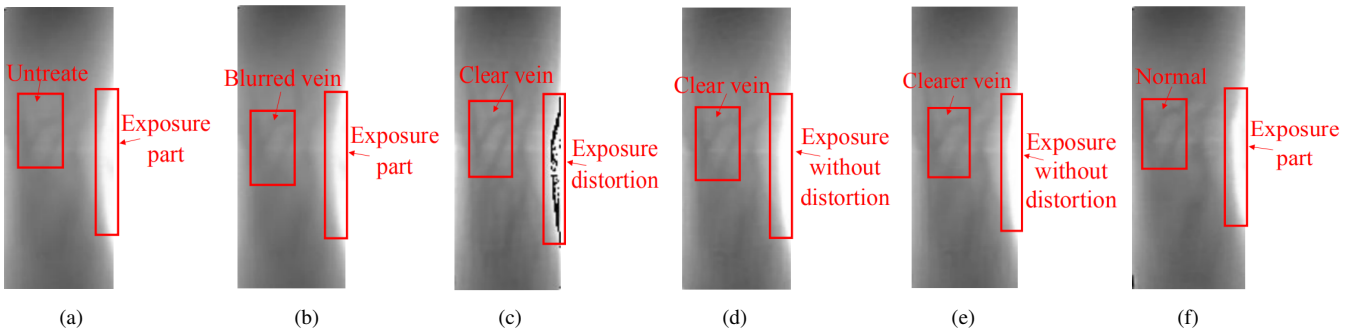

Fig. 9. Deblurred finger vein images restored by four different deblurring methods. (a): Untreated real local blurred finger vein image captrued by excessive pressure. (b): 24-layer DeblurGAN [16] generator network trained with single-blur-degree training dataset (c): The proposed 26-layer generator network trained with single-blur-degree training dataset. (d): The proposed 26-layer generator network constrained by NBP texture loss and trained with single-blur-degree training dataset. (e): The proposed 26-layer generator network constrained by NBP texture loss and trained with polymorphic training dataset. (f): Normal clear finger vein image.

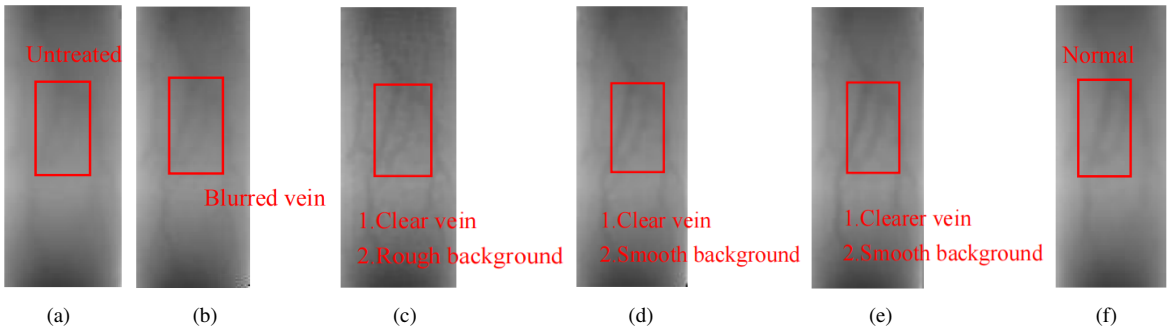

Fig. 10. Deblurred finger vein images restored by four different deblurring methods. (a): Untreated real global blurred finger vein image captrued in low temperature. (b): 24-layer DeblurGAN [16] generator network trained with single-blur-degree training dataset (c): The proposed 26-layer generator network trained with single-blur-degree training dataset. (d): The proposed 26-layer generator network constrained by NBP texture loss and trained with single-blur-degree training dataset. (e): The proposed 26-layer generator network constrained by NBP texture loss and trained with polymorphic training dataset. (f): Normal clear finger vein image.

1) Real Local Blur Caused by Venous Compression: Finger vein recognition systems are based on finger vein texture features, hence, a clear and continuous finger vein texture is critical. Fig. 9 (a) is the input blurred finger vein image captured by excessive pressure, where blurred vein texture (low discrimination between veins and background) can be clearly observed. Fig. 9 (b)∼(e) is the deblurred image of finger vein with four different deblurring network models. Fig. 9 (f) is the image of finger vein captrued by normal pressure placement. Fig. 9 (b) is the finger vein image deblurred by the 24-layer DeblurGAN [16] generator network. Comparing Fig. 9 (a) with Fig. 9 (b), it can be seen that the vein texture in Fig. 9 (b) still exhibits blurriness. The restored finger vein image by the proposed 26-layer generator network is shown in Fig. 9 (c). Compared with Fig. 9 (b), the vein texture clearness is significantly improved, but there exists a certain degree of distortion in the high exposure part of the image edge. Furthermore, by using the 26-layer generator network constrained by NBP texture loss, one can see from Fig. 9(d) that the abnormal exposure distortion is removed. Finally, the deblurred vein image obtained by the 26-layer generator network constrained by NBP texture loss and trained with the polymorphic blurred training dataset is presented in Fig. 9 (e). One can see that the vein texture of the deblurred image is much clearer than Fig. 9 (d), and it is highly similar to the vein texture structure in the clear image shown by Fig. 9 (f).

2) Real Global Blur Caused by Venous Contraction: Fig. 10 (a) is the input blurred finger vein image due to excessive pressure, where one can see a certain degree of vein texture discontinuity by comparing with the original clear finger vein image (as shown in Fig. 10 (f)). Fig. 10 (b)∼(e) are the deblurred finger vein images of four different deblurring network models. Fig. 10 (f) is a finger vein image captured when the finger temperature is normal in summer. Fig. 10 (b) is the finger vein image deblurred by the 24-layer DeblurGAN [16] generator network. Comparing Fig. 10 (a) and Fig. 10 (b), it can be seen that the deblurring effect of DeblurGAN is not obvious, and the deblurred image has a blurred vein texture. The deblurred image produced by the proposed 26-layer generator network is given in Fig. 10 (c), where clearer vein texture can be observed, but there is some rough background as well. The deblurred image (see Fig. 10 (d)) produced by the proposed 26-layer generator network constrained by NBP texture loss has higher fidelity and its background is smoother than Fig. 10 (c), closer to the practical finger vein clear image. However, the training dataset contains a small amount of blur types and the generalization ability is limited. After trained with the polymorphic blurred training dataset, the restored finger vein image by the proposed deblurring NB-GAN model as shown in Fig. 10 (e) has clearer

TABLE V
COMPARISON OF PNSR AND SSIM UNDER DIFFERENT DEBLURRING METHODS

Deblurring algorithm	PSNR	SSIM
Untreated	19.33	0.8616
DeblurGAN [16] with single-blur-degree training set	25.55	0.9614
DeblurGAN [16] with polymorphic training set	28.89	0.9759
NB-GAN with single-blur-degree training set	27.36	0.9531
NB-GAN with NBP loss and single-blur-degree training set	28.99	0.9768
NB-GAN with NBP loss and polymorphic training set	30.42	0.9885

TABLE VI
p-VALUES RETURNED FROM KRUSKAL-WALLS TEST

NB-GAN with NBP loss and polymorphic training set versus	p-value	
	PSNR	SSIM
Untreated	1.75e-10	4.77e-12
DeblurGAN [16] with single-blur-degree training set	7.42e-5	6.67e-8
DeblurGAN [16] with polymorphic training set	1.60e-2	2.40e-3
NB-GAN with single-blur-degree training set	4.04e-2	6.60e-4
NB-GAN with NBP loss and single-blur-degree training set	7.81e-4	3.90e-3

vein texture than Fig. 10 (d) and is identical to Fig. 10 (f).

B. Evaluation of Image Quality

In this paper, PSNR [18] and SSIM [18] are used as the quality criteria for comparing between NB-GAN and DeblurGAN [16]. PSNR evaluates the image quality by measuring the error between the corresponding pixels of two images. The PSNR value function is defined as follows,

$$\begin{aligned} PSNR &= 10 \cdot \lg(\frac{255}{MSE_{\mathrm{NB}}}) \\ MSE_{\mathrm{NB}} &= \frac{1}{TRCM}\sum_{m=1}^{M}(Img^{m}_{\mathrm{clear}} - Img^{m}_{\mathrm{deblur}})^2 \end{aligned} \tag{15}$$

where $Img^{m}_{\mathrm{deblur}}$ represents the m^{th} deblurring finger vein imgae, $PSNR$ represents the PSNR value in dB. The larger the PSNR value, the higher the quality of the restored image is. SSIM uses mean value as brightness estimation, standard deviation as contrast estimation, and covariance as a measure of structural similarity. The SSIM value function is calculated as follows,

$$\begin{aligned} SSIM &= \frac{1}{M}\sum_{m=1}^{M} SSIM^{m}_{\mathrm{B}} \cdot SSIM^{m}_{\mathrm{C}} \cdot SSIM^{m}_{\mathrm{S}} \\ SSIM^{m}_{\mathrm{B}} &= \frac{2\mu(Img^{m}_{\mathrm{clear}})\mu(Img^{m}_{\mathrm{deblur}}) + Cnt_1}{\mu^2(Img^{m}_{\mathrm{clear}}) + \mu^2(Img^{m}_{\mathrm{deblur}}) + Cnt_1} \\ SSIM^{m}_{\mathrm{C}} &= \frac{2\sigma(Img^{m}_{\mathrm{clear}})\sigma(Img^{m}_{\mathrm{deblur}}) + Cnt_2}{\sigma^2(Img^{m}_{\mathrm{clear}}) + \sigma^2(Img^{m}_{\mathrm{deblur}}) + Cnt_2} \\ SSIM^{m}_{\mathrm{S}} &= \frac{2\xi(Img^{m}_{\mathrm{clear}}, Img^{m}_{\mathrm{deblur}}) + Cnt_3}{\sigma(Img^{m}_{\mathrm{clear}})\sigma(Img^{m}_{\mathrm{deblur}}) + Cnt_3} \\ Cnt_1 &= (255K_1)^2, Cnt_2 = (255K_2)^2, Cnt_3 = \frac{Cnt_2}{2} \end{aligned} \tag{16}$$

where $\mu(*)$, $\sigma(*)$, $\xi(*)$ stand for the mean functions, variance functions, and covariance functions, respectively. The $SSIM$ represents the SSIM value. The maximum $SSIM$ is 1. The larger the SSIM value, the higher the similarity between the two images. After deblurring all the images within the synthetic blurred testing dataset, the PSNR and SSIM values are calculated based on the 1440 deblurred testing images and the corresponding clear images. Thus, there are a total of 1440 values for each measure, and the average results are reported in Table V.

Table V one can see that, the PSNR value of images restored by the proposed 26-layer generator network is higher than the 24-layer DeblurGAN [16], but the SSIM value is lower. After trained with polymorphic training dataset, the generator of DeblurGAN can learn more comprehensive mapping information, leading to better performance in terms of higher PSNR and SSIM values. This suggests that the deblurred finger vein images generated by the proposed model are closer to the real clear vein images, but there also exist some issues such as special point distortion and rough background that affect the structure similarity. After using the 26-layer generator network constrained by NBP texture loss, the SSIM value increases to 0.9768, showing that by using NBP texture loss to constrain the proposed model, the fidelity of the generated images is improved. Finally, both PSNR and SSIM values are further improved after using the polymorphic training dataset for training, suggesting that the generalization ability of the proposed network is greatly improved, leading to a better deblurring performance.

To examine whether the performance improvement of the proposed NB-GAN trained with polymorphic training dataset over other methods in terms of PSNR and SSIM was of statistical significance, Kruskal-Wallis tests [25] are conducted in this paper. p-values returned from the statistical tests are presented in Table VI. From Table VI one can see that all the returned p-values are bellowing the statistical hypothesis level $\alpha = 0.05$, suggesting that the performance improvement of the proposed method is statistically significant.

C. Evaluation of Recognition Performance

This paper uses the NBP [17] recognition algorithm to evaluate the performance recognition of deblurred images. During the image matching process, image enhancement [26] is firstly performed on each pair of candidate images. Then NBP features of the two images are extracted. The Hamming

distance of the NBP features of the two images is taken as the feature matching value. If the matching value is less than a given threshold t, it is determined that the two images are from the same finger. This study uses the standard False Acceptance Rate (FAR) and False Rejection Rate (FRR) as the performance measures. Typically, the lower the FRR, the better the recognition performance. Since the FAR is expected to be as small as possible in a high-security scenario [27], we only consider the FRR rates in the case of FAR$=0\%$. The FRR rates function is defined as follows,

$$FRR = 1 - \frac{N_{\mathrm{s}}}{N_{\mathrm{t}}} \times 100\% \tag{17}$$

where N_{s} represents number of images successfully recognized during the recognition process; N_{t} represents the total number of images involved. The Receiver Operating Characteristic (ROC) curves in Fig. 11, Fig. 12 and Fig. 13 show that the FRR of synthetic blurred testing dataset, real local blurred testing dataset generated from finger vein compression and real global blurred testing dataset generated from finger vein

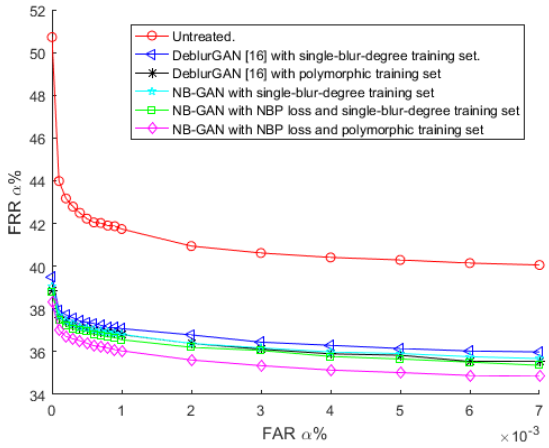

Fig. 11. ROC curve of the synthetic blurred finger vein testing dataset under different deblurring methods

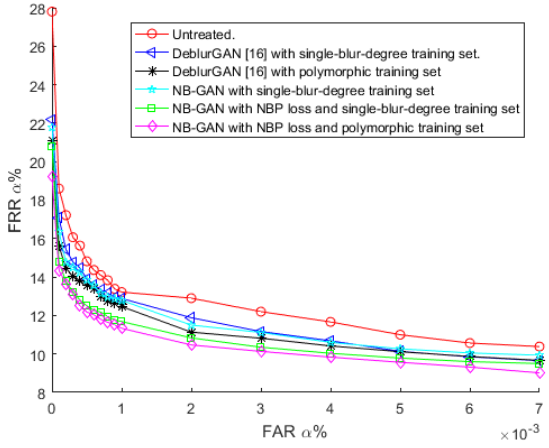

Fig. 12. ROC curve of the real local blurred venous compression testing dataset under different deblurring methods

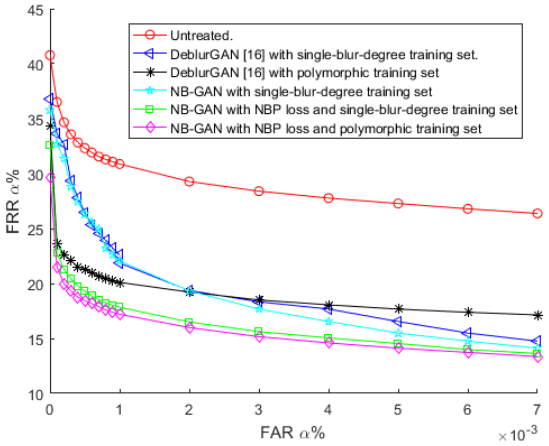

Fig. 13. ROC curve of the real global blurred vein contraction testing dataset under different deblurring methods

contraction are as high as 50.72%, 27.8%, 40.78% without processing. It shows that the blurriness of finger vein image will seriously affect the feature extraction, resulting in the degradation of recognition performance. After being processed by DeblurGAN deblurring algorithm [16], the FRR rates drop to 39.51%, 22.18%, 36.68%, and the recognition performance is improved to a certain extent. However, since the restored finger vein image still has blurred vein texture, the recognition rate is not improved much. After trained with the polymorphic blurred dataset, the generalization ability of the DeblurGAN model is enhanced and the FRR rates decreased to 38.88%, 21.10%, and 34.34% on the three testing datasets, respectively. The FRR rates dropped to 39.06%, 21.78%, and 35.78% on the three testing datasets, respectively, thanks to richer vein features extracted by the proposed 26-layer generator network. This shows that the texture clearness of the deblurred finger vein images is enhanced, but the deblurred images still suffer from a certain degree of defect, such as abnormal exposure point distortion and rough background. With the 26-layer generator network constrained by NBP texture loss, which can help the model to extract highly accurate vein texture structural features from images, the FRR rates on the three testing datasets drops to 38.79%, 20.77%, and 32.63%. Which suggests that the defect of rough background and distortion is solved, and the fidelity of the deblurred finger vein image is improved. Finally, the polymorphic blurred training dataset is used to train the network model for improving the generalization ability of generator network, enabling the model to learn more comprehensive mapping information from the blurred finger vein image to the clear finger vein image. The FRR rates on three datasets drop to 38.33%, 19.25%, and 29.61% further.

From Fig. 11, Fig. 12, and Fig. 13, it can be found that the proposed NB-GAN can achieve better performance on the three testing datasets than DeblurGAN. On the other hand, one may notice that using the polymorphic training dataset for training can enhance the performances of both NB-GAN and DeblurGAN, demonstrating the effectiveness and validity of the blurriness modelling and augmentation method proposed

in this paper.

Through the above experimental analysis, one may conclude that the NB-GAN proposed in this paper show better deblurring performance on finger vein images than DeblurGAN. The deblurred finger vein image generated by NB-GAN has clearer vein contours and less noisy background, resulting in better recognition accuracy.

VII. Conclusion

This paper proposed a finger vein deblurring approach based on a 26-layer NB-GAN. Starting with the analysis of different types of blurriness in the finger vein images captured in real-world applications, we firstly introduced the mathematical model of local blurriness and global blurriness. Based on this, a polymorphic blur training set is created from clear images for network training. To help the model retain more vein texture feature information, residual jump connections were further added to both sides of the residual module of the network. The experimental results show that, compared with the widely used DeblurGAN [16] deblurring model, the proposed NB-GAN approach has stronger deblurring ability and can restore higher quality vein structures from blurred finger vein images.

On the other hand, we have to admit that this study does not provide a scientific definition for the standard of judgement between blurred images and clear images. Although there exist a few approaches to directly measure the degree of blurriness of the images, we did not explore this direction in our study at this moment. As future works, we will further involve such blurriness measures in the loss functions for network training.

VIII. Acknowledgements

The authors would like to express the sincere appreciation to the editor and anonymous reviewers for their insightful comments, which greatly improve the quality of this paper. This work was supported in part by the National Natural Science Foundation of China under Grant 61976120 and by the Natural Science Foundation of Jiangsu Province under Grant BK20191445, and sponsored by Qing Lan Project of Jiangsu Province.

References

[1] D. Ezhilmaran and P. R. B. Joseph, "Fuzzy inference system for finger vein biometric images," in *Proc. Int. Conf. Inventive Systems and Control. (ICISC)*, pp. 1-4, 2017.

[2] C. Hsia, "New Verification Strategy for Finger-Vein Recognition System, *IEEE Sensors Journal.*, vol. 18, no. 2, pp. 790-797, Jan. 2018.

[3] T. H. Kim and K. M. Lee, "Segmentation-Free Dynamic Scene Deblurring," in *Proc. IEEE Conf. Comput. Vis. Pattern Recognit. (CVPR)*, pp. 2766-2773, 2014.

[4] A. Gupta, N. Joshi, C. Lawrence Zitnick, K. Daniilidis, P. Maragos, and N. Paragios, "Single image deblurring using motion density functions," *Lecture Notes in Computer Science.*, vol. 6311, pp. 171-184, 2010.

[5] R. Fergus, B. Singh, A. Hertzmann, *et al*, "Removing camera shake from a single photograph," *Association for Computing Machinery.*, vol. 26, no. 3, pp. 787-794, 2006.

[6] L. Xu, S. Zheng, and J. Jia, "Unnatural 10 sparse representation for natural image deblurring," in *Proc. IEEE Conf. Comput. Vis. Pattern Recognit. (CVPR)*, pp. 1107-1114, 2013.

[7] O. Whyte, J. Sivic, A. Zisserman, *et al.*, "Non-uniform deblurring for shaken images," in *Proc. IEEE Conf. Comput. Vis. Pattern Recognit. (CVPR)*, vol. 98, no. 2, pp. 168-186, 2012.

[8] J. Sun, W. Cao, Z. Xu, *et al.*, "Learning a convolutional neural network for non-uniform motion blur removal," in *Proc. IEEE Conf. Comput. Vis. Pattern Recognit. (CVPR)*, pp. 1125-1134, 2017.

[9] D. Gong, J. Yang, L. Liu, *et al.*, "From motion blur to motion flow:a deep learning solution for removing heterogeneous motion blur," in *Proc. IEEE Conf. Comput. Vis. Pattern Recognit. (CVPR)*, pp. 2319-2328, 2017.

[10] S. Nah, H. T. Kim, and M. K. Lee, "Deep multi-scale convolutional neural network for dynamic scene deblurring," in *Proc. IEEE Conf. Comput. Vis. Pattern Recognit. (CVPR)*, pp. 257-265, 2017.

[11] M. Noroozi, P. Chandramouli, and P. Favaro, "Motion debluring in the wild," *Lecture Notes in Computer Science.*, vol. 10496, pp. 65-77, 2017.

[12] S. Ramakrishnan, S. Pachori, A. Gangopadhyay, *et al.*, "Deep generative filter for motion debluring," in *Proc. IEEE Int. Conf. Comput. Vis. Workshops. (ICCVW)*, pp. 2993-3000, 2017.

[13] I. Goodfellow, J. Pouget-Abadie, M. Mirza, *et al.*, "Generative adversarial nets," in *Proc. 27th Int. Conf. on Neural Information Processing Systems.*, pp. 2672-2680, 2014.

[14] Q. Li *et al.*, "AF-DCGAN: Amplitude Feature Deep Convolutional GAN for Fingerprint Construction in Indoor Localization Systems," in *IEEE Transactions on Emerging Topics in Computational Intelligence*, vol. 5, no. 3, pp. 468-480, June 2021.

[15] Z. Pan *et al.*, "Loss Functions of Generative Adversarial Networks (GANs): Opportunities and Challenges," in *IEEE Transactions on Emerging Topics in Computational Intelligence*, vol. 4, no. 4, pp. 500-522, Aug. 2020.

[16] O. Kupyn, V. Budzan, M. Mykhailych, *et al.*, "Deblurgan:Blind motion deblurring using conditional adversarial networks," in *Proc. IEEE Conf. Comput. Vis. Pattern Recognit. (CVPR)*, pp. 8183-8192, 2018.

[17] I. Hamouchene and S. Aouat, "A cognitive approach for texture analysis using neighbors-based binary patterns," in *Proc. IEEE 13th Int. Conf. Cogn. Informatics and Cogn. Computing. (ICCI-CC)*, pp. 94-99, 2014.

[18] A. Hore and D. Ziou, "Image quality metrics:PSNR vs. SSIM," in *Proc. 20th Int. Conf. Pattern Recognit. (ICPR)*, pp. 2366-2369, August, 2010.

[19] G. Gong and K. Zhang, "Local Blurred Natural Image Restoration Based on Self-Reference Deblurring Generative Adversarial Networks," in *Proc. IEEE Int. Conf. Signal and Image Processing Applications. (ICSIPA)*, pp. 231-235, 2018.

[20] H. Yang, L. Shen, Y. Yao, H. Wang and G. Zhao, "Finger Vein Image Inpainting With Gabor Texture Constraints," *IEEE Access*, vol. 8, pp. 83041-83051, 2020.

[21] W. You, W. Zhou, J. Huang, F. Yang, Y. Liu and Z. Chen, "A bilayer image restoration for finger vein recognition", *Neurocomputing*, vol. 348, pp. 54-65, Jul. 2019.

[22] P. Isola, Y. J. Zhu, T. Zhou, *et al.*, "Image-to-image translation with conditional adversarial networks," in *Proc. IEEE Conf. Comput. Vis. Pattern Recognit. (CVPR)*, pp. 1125-1134, 2017.

[23] X. Mao, Q. Li, H. Xie, R. Y. K. Lau, Z. Wang, and S. P. Smolley, "Least Squares Generative Adversarial Networks," in *Proc. IEEE Int. Conf. Comput. Vis. (ICCV)*, pp. 2813-2821, 2017.

[24] C. Verma, V. Stoffov, Z. Ills, S. Tanwar, and N. Kumar, "Machine Learning-Based Students Native Place Identification for Real-Time," *IEEE Access*, vol. 8, pp. 130840-130854, 2020.

[25] Z. Wang and Z. Xie, "Infrared face recognition based on local binary patterns and Kruskal-Wallis test," in *Proc. IEEE/ACIS Int. Conf. on Computer and Information Science (ICIS)*, pp. 185-188, 2014.

[26] D. L. Hang, *et al.*, "Combination of contrast limited adaptive histogram equalisation and discrete wavelet transform for image enhancement," *IET Image Processing.*, vol. 9, no. 10, pp. 908-915, 2015.

[27] R. Ramachandra, K. B. Raja, S. K. Venkatesh, and C. Busch, "Design and Development of Low-Cost Sensor to Capture Ventral and Dorsal Finger Vein for Biometric Authentication," *IEEE Sensors Journal.*, vol. 19, no. 15, pp. 6102-6111, Aug. 2019.

Jing He is currently pursuing the masters degree with the School of Communication Engineering, Hangzhou Dianzi University. His research interests include biometric recognition and image processing by deep learning.

Lei Shen received the B.Eng. and Ph.D. degrees in electronic engineering from Zhejiang University, Hangzhou, China, in 2002 and 2007, respectively. From 2014 to 2015, he was a Visiting Scholar with the Department of Electrical and Computer Engineering, Stevens Institute of Technology, Hoboken, NJ, USA. He is currently a Professor with the College of Communication Engineering, Hangzhou Dianzi University, Hangzhou. His research interests include vein image processing and signal processing.

Yudong Yao (Fellow, IEEE) received the B.Eng. and M.Eng. degrees in electrical engineering from the Nanjing University of Posts and Telecommunications, Nanjing, China, in 1982 and 1985, respectively, and the Ph.D. degree in electrical engineering from Southeast University, Nanjing, in 1988. From 1987 to 1988, he was a Visiting Student with Carleton University, Ottawa, ON, Canada. From 1989 to 2000, he was with Carleton University, Spar Aerospace Ltd., Montreal, QC, Canada, and Qualcomm Inc., San Diego, CA, USA. Since 2000, he has been with the Stevens Institute of Technology, Hoboken, NJ, USA, where he is currently a Professor and the Chair of the Department of Electrical and Computer Engineering. He holds one Chinese patent and over 13 U.S. patents. His research interests include wireless communications, cognitive radio, machine learning, and deep learning techniques. He served as an Associate Editor for the IEEE COMMUNICATIONS LETTERS, from 2000 to 2008, and the IEEE TRANSACTIONS ON VEHICULAR TECHNOLOGY, from 2001 to 2006. He also served as an Editor for the IEEE TRANSACTIONS ON WIRELESS COMMUNICATIONS, from 2001 to 2005. For his contributions to wireless communications systems, he was elected as the National Academy of Inventors, in 2015, and the Canadian Academy of Engineering, in 2017.

Huaxia Wang (Member, IEEE) received the B.Eng. degree in information engineering from Southeast University, Nanjing, China, in 2012, and the Ph.D. degree in electric engineering from the Stevens Institute of Technology, Hoboken, NJ, USA, in 2018. From 2016 to 2017, he was a Research Intern with the Mathematics of Networks and Systems Research Department and Nokia Bell Labs, Murray Hill, NJ, USA. He joined Futurewei Technologies Inc., Bridgewater, NJ, USA, in 2018. He is currently a Co-Professor with the Oklahoma State University, Stillwater, OK, USA. He has published more than 15 articles in premium conferences and peer-reviewed journals, including ICLR, the IEEE JOURNAL ON SELECTED AREAS IN COMMUNICATIONS, the IEEE TRANSACTIONS ON WIRELESS COMMUNICATIONS, the IEEE TRANSACTIONS ON NEURAL NETWORKS AND LEARNING SYSTEMS, the IEEE TRANSACTIONS ON VEHICULAR TECHNOLOGY, and so on. His research interests include image processing, wireless communications, cognitive radio networks, reinforcement learning, and deep learning. He was a recipient of the Outstanding Ph.D. Dissertation Award in electrical engineering and the Edward Peskin Award with the Stevens Institute of Technology, in 2018.

Guodong Zhao received the Ph.D. degree in communication and information system from the Chinese Academy of Sciences, Shanghai, China, in 2008. He is currently a Chief Technology Officer with Top Glory Tech Limited Company, China. His current research interest includes biometric identification technology.

Xiaowei Gu received the PhD degree in computer science from Lancaster University, U.K.,and the MEng degree in communication and information systems and the BEng degree in communicationengineering from Hangzhou Dianzi University, China. Dr. Gu is currently a Lecturer in Computer Science at the Department of Computer Science, Aberystwyth University, U.K. His major research interests include machine learning, data analytics and signal processing.

Weiping Ding (M16-SM19) received the Ph.D. degree in Computation Application, Nanjing University of Aeronautics and Astronautics (NUAA), Nanjing, China, in 2013. From 2014 to 2015, he is a Postdoctoral Researcher at the Brain Research Center, National Chiao Tung University (NCTU), Hsinchu, Taiwan. In 2016, He was a Visiting Scholar at National University of Singapore (NUS), Singapore. From 2017 to 2018, he was a Visiting Professor at University of Technology Sydney (UTS), Ultimo, NSW, Australia. He is currently a professor with the School of Information Science and Technology, Nantong University, Nantong, China. His research interests include deep neural networks, multimodal machine learning, granular data mining, uncertainty modeling in big data, co-evolutionary algorithm, and medical images analysis. He has published more than 100 journal papers, including IEEE T-FS, T-NNLS, T-CYB, T-SMCS, T-BME, T-EVC, T-II, T-ETCI, T-CDS, and T-ITS. He serves on the Editorial Board of Information Fusion, Applied Soft Computing, and served/serves as an Associate Editor of IEEE Transactions on Fuzzy Systems, Information Sciences, Neurocomputing, Swarm and Evolutionary Computation, Engineering Applications of Artificial Intelligence, IEEE/CAA Journal of Automatica Sinica, etc. He is the Leading Guest Editor of Special Issues in several prestigious journals, including IEEE Transactions on Evolutionary Computation, IEEE Transactions on Fuzzy Systems, and so on.